Available on the CERN CDS information server **CMS PAS HIG-13-021**

CMS Physics Analysis Summary

Contact: cms-pag-conveners-higgs@cern.ch 2013/11/01

Search for MSSM Neutral Higgs Bosons Decaying to Tau Pairs in pp Collisions

The CMS Collaboration

Abstract

A search for neutral Higgs bosons in the minimal supersymmetric extension of the standard model (MSSM) decaying to tau pairs is performed using events recorded by the CMS experiment at the LHC in 2011 and 2012 at a center-of-mass energy of 7 TeV and 8 TeV respectively. The dataset corresponds to an integrated luminosity of 24.6 fb^{-1}, with 4.9 fb^{-1} at 7 TeV and 19.7 fb^{-1} at 8 TeV. To enhance the sensitivity to neutral MSSM Higgs bosons, the search includes the case where the Higgs boson is produced in association with a b-quark jet. No excess is observed in the tau-pair invariant-mass spectrum. Exclusion limits in the MSSM parameter space of M_A and $\tan\beta$ in the m_h^{max} scenario are presented. Upper limits on the cross section times branching ratio for gluon-fusion and b-associated Higgs production are also given.

1 Introduction

Experimental evidence from a large number of high energy experiments has shown an overwhelming success of the Standard Model (SM) of fundamental interactions, although some questions remain unanswered like the origin of mass of elementary particles. In the SM [1–3], this is achieved via the Higgs mechanism [4–9], which also predicts the existence of a scalar Higgs boson. However, the SM Higgs boson suffers from quadratically divergent self-energy corrections at high energy. Numerous extensions to the SM have been proposed to address these divergences. In the model of supersymmetry (SUSY) [10, 11] , a symmetry between fundamental bosons and fermions, a cancellation of these divergences occurs. The Higgs sector of the minimal supersymmetric standard model (MSSM) [12, 13] has two scalar doublets which results in five physical Higgs bosons: a light and heavy CP-even h and H, the CP-odd A and the charged Higgs boson $H^{\pm}$. At lowest order the Higgs sector can be expressed in terms of two parameters which are usually chosen as tanβ, the ratio of the two vacuum expectation values, and the mass of the CP-odd boson, M_A.

The dominant neutral MSSM Higgs boson production mechanism is the gluon-fusion process, $gg \to h, H, A$, for small and moderate values of tanβ. At large values of tanβ the b-associated production is the dominant contribution, due to the enhanced bottom Yukawa coupling. In the region of large tanβ the branching ratio to tau leptons is enhanced, making the search for neutral MSSM Higgs bosons in the di-τ final state of particular interest.

This Summary reports a search for neutral MSSM Higgs bosons in pp collisions at $\sqrt{s} = 7$ TeV and 8 TeV at the LHC. The data were recorded by the Compact Muon Solenoid experiment (CMS) [14] in 2011 and 2012 and correspond to an integrated luminosity of 24.6 fb^{-1}, with 4.9 fb^{-1} at 7 TeV and 19.7 fb^{-1} at 8 TeV. Five different $\tau\tau$ final states are studied: eτ_h, $\mu\tau_h$, eμ, $\mu\mu$ and $\tau_h\tau_h$, where τ_h denotes a hadronic decay of a τ. These results are an extension of a previous search by the CMS experiment [15] and are similar to those performed by the the ATLAS experiment [16], the Tevatron [17–19], and are complimentary to the MSSM Higgs search at LEP [20].

Traditionally, searches for MSSM Higgs bosons are expressed in terms of benchmark scenarios where the lowest-order parameters tanβ and M_A are varied, while fixing the other parameters that enter through radiative corrections to certain benchmark values. In this study, the m_h^{max} scenario [21, 22] is used as it yields conservative expected limits in the tanβ and M_A plane.

Recently the CMS and ATLAS experiments have reported the observation of a new boson with mass in the range 125-126 GeV [23, 24]. An indication that this new boson decays into tau pairs has recently been reported by CMS [25]. If the new boson is interpreted as the light scalar MSSM Higgs h, part of the tanβ and M_A parameter space in the m_h^{max} scenario is excluded. However, changes in the stop mixing parameter open up a large region of the allowed parameter space [26, 27].

In this report, the results are interpreted both in the context of the MSSM m_h^{max} scenario and also in a model independent way, in terms of upper limits on $\sigma \cdot \text{BR}(\Phi \to \tau\tau)$ for gluon-fusion and b-associated neutral Higgs boson production, where we denote by Φ any of the three neutral MSSM Higgs bosons.

2 Trigger and Event Selection

The trigger selection requires a combination of electron, muon and tau trigger objects [28–30]. The identification criteria and transverse momentum thresholds of these objects were progres-

sively tightened as the LHC instantaneous luminosity increased over the data-taking period.

A particle-flow algorithm [31–33] is used to combine information from all CMS subdetectors to identify and reconstruct individual particles in the event, namely muons, electrons, photons, and charged and neutral hadrons. From the resulting particle list jets, hadronically decaying taus, and missing transverse energy ($\not\!\!E_{\mathrm{T}}$), defined as the magnitude of the vector sum of the transverse momenta, are reconstructed. The jets are reconstructed using the anti-k_T jet algorithm [34, 35] with a distance parameter of $R = 0.5$. Hadronically-decaying taus are reconstructed using the hadron plus strips (HPS) algorithm, which considers candidates with one charged pion and up to two neutral pions or three charged pions [36]. To tag jets coming from b-quark decays the Combined Secondary Vertex (CSV) algorithm is used. This algorithm is based on the reconstruction of secondary vertices, together with track-based lifetime information [37].

Events in the eτ_h ($\mu\tau_h$) final state are required to contain an electron of $p_{\mathrm{T}} > 20$ GeV (muon $p_{\mathrm{T}} > 17$ GeV) and $|\eta| < 2.1$ plus an oppositely charged τ_h of $p_{\mathrm{T}} > 20$ GeV and $|\eta| < 2.3$. The p_{T} thresholds for electrons (muons) are increased to 24 GeV (20 GeV) in the 2012 dataset, following the raise in trigger thresholds at higher instantaneous luminosity. To reduce the contamination of $\mathrm{Z} \to$ ee, $\mu\mu$ background, events with two electrons or muons of $p_{\mathrm{T}} > 15$ GeV, opposite charge and passing loose isolation criteria are rejected. $\mathrm{Z} \to$ ee background in the eτ_h final state is further suppressed by requiring $\not\!\!E_{\mathrm{T}} > 25$ GeV. In the eμ and $\mu\mu$ final states events with two oppositely charged leptons are selected, where the highest-p_{T} lepton is required to have $p_{\mathrm{T}} > 20$ GeV and the second-highest-p_{T} lepton $p_{\mathrm{T}} > 10$ GeV. Muons with $|\eta| < 2.1$ and electrons with $|\eta| < 2.3$ are used. The large background arising from $\mathrm{Z} \to \mu\mu$ events in the $\mu\mu$ channel is removed by a multivariate *Boosted Decision Tree* (BDT) discriminator. In the $\tau_h\tau_h$ final states events with two oppositely charged hadronic taus with $p_{\mathrm{T}} > 45$ GeV and $|\eta| < 2.1$ are selected.

An average of 10 (20) proton-proton interactions occurred per LHC bunch crossing in 2011 (2012), making the reconstruction of physics objects challenging. For each reconstructed collision vertex the sum of the p_{T}^2 of all tracks associated to the vertex is computed and the one with the largest value is taken as the primary collision vertex. In order to mitigate the effects of pile–up on the reconstruction of $\not\!\!E_{\mathrm{T}}$, a multivariate regression correction is used where the inputs are separated in those components coming from the primary vertex and those which are not [38]. The correction improves the $\not\!\!E_{\mathrm{T}}$ resolution in $\mathrm{Z} \to \mu\mu$ events by roughly a factor of two in case 25 additional pile-up events are present.

Taus from Higgs boson decays are expected to be isolated in the detector, while leptons from heavy-flavor (c and b) decays and decays in flight are expected to be found inside jets. A measure of isolation is used to discriminate the signal from the QCD multijet background, based on the charged hadrons, photons, and neutral hadrons falling within a cone around the lepton momentum direction. A correction is applied to the isolation to reduce the effects of pile-up. For charged particles, only those associated with the primary vertex are considered and for neutral particles, a correction is applied by subtracting the energy deposited in the isolation cone by charged particles not associated with the primary vertex, multiplied by a factor of 0.5 which approximately corresponds to the ratio of neutral to charged hadron production in the hadronization process of pile-up interactions. An η, p_{T}, and lepton-flavor dependent threshold on the isolation variable of less than roughly 10% of the candidate p_{T} is applied.

To correct for the contribution to the jet energy due to pile-up, a median energy density (ρ) is determined event by event. The pile-up contribution to the jet energy is estimated as the product of ρ and the area of the jet and subsequently subtracted from the jet transverse energy [39].

In the fiducial region for jets of $|\eta| < 4.7$, jet energy corrections are also applied as a function of the jet E_{T} and η [40].

In order to reject events coming from W+jets background a dedicated selection is applied. In the eτ_h and $\mu\tau_h$ final states, the transverse mass of the electron or muon and the $\not\!\!E_{\mathrm{T}}$, $M_T = \sqrt{2p_{\mathrm{T}}\not\!\!E_{\mathrm{T}}(1-\cos\Delta\phi)}$, is required to be less than 30 GeV, where p_{T} is the lepton transverse momentum and $\Delta\phi$ is the difference in ϕ of the lepton and $\not\!\!E_{\mathrm{T}}$ vector. In the eμ final states, a discriminator is formed by considering the bisector of the directions of the visible tau decay products transverse to the beam direction, denoted as the ζ axis. From the projections of the visible decay product momenta and the $\not\!\!E_{\mathrm{T}}$ vector onto the ζ axis, two values are calculated: $P_\zeta = (p_{\mathrm{T},1} + p_{\mathrm{T},2} + \not\!\!E_{\mathrm{T}}) \cdot \zeta \quad ; \quad P_\zeta^{\mathrm{vis}} = (p_{\mathrm{T},1} + p_{\mathrm{T},2}) \cdot \zeta$, where $p_{\mathrm{T},1}$ and $p_{\mathrm{T},2}$ indicate the transverse momentum of two reconstructed leptons. eμ events are selected with $P_\zeta - 1.85 \cdot P_\zeta^{\mathrm{vis}} > -20$ GeV.

To further enhance the sensitivity of the search for Higgs bosons, the sample of selected events is split into two mutually exclusive categories:

- **B-Tag:** This event category is intended to exploit the production of Higgs bosons in association with b-quarks which is enhanced in the MSSM. At least one b-tagged jet with $p_{\mathrm{T}} > 20$ GeV is required and not more than one jet with $p_{\mathrm{T}} > 30$ GeV.
- **No-B-Tag:** This event category is mainly sensitive to the gluon-fusion Higgs production mechanism. Events are required to have no b-tagged jets with $p_{\mathrm{T}} > 20$ GeV.

The observed number of events for each category, as well as the expected number of events from various background processes, are shown in Tables 1– 4 together with expected signal yields and efficiencies.

The largest source of background events comes from $Z \to \tau\tau$, which is estimated using a sample of $Z \to \mu\mu$ events where the reconstructed muons are replaced by the reconstructed particles from simulated tau decays. The normalization for this process is determined from the measurement of the $Z \to \mu\mu$ yield in data. Another significant source of background is QCD multijet events. QCD events may contribute to the $\tau_h\tau_h$ (eτ_h and $\mu\tau_h$) channel in case two jets are misidentified as hadronic tau decays (one jet is misidentified as an isolated electron or muon, and a second jet as τ_h). The QCD background contribution in the $\tau_h\tau_h$ channel is estimated by measuring, in a control region, the probability for jets to pass hadronic tau identification criteria and applying these probabilities as weights to events which pass all event selection criteria except tau identification requirements. In the eτ_h and $\mu\tau_h$ channels the rate of QCD background is estimated using the number of observed same-charge tau pair events. Events from W+jets in which there is a jet misidentified as a τ_h are another sizeable source of background in the eτ_h and $\mu\tau_h$ channels. The rate of this background is estimated using a control region of events with large transverse mass. Other background processes include $\mathrm{t\bar{t}}$ production and $Z \to ee/\mu\mu$ events, particularly in the eτ_h channel, as the the probability for electrons to be misidentified as τ_h amounts to 1–2%. In the eμ final state, the W+jets and multijet background events are obtained by measuring the number of events with one good lepton and a second one which passes relaxed selection criteria, but fails the nominal lepton selection. This sample is extrapolated to the signal region using the efficiencies for such loose lepton candidates to pass the nominal lepton selection. These efficiencies are measured in data using observed multijet events. The shape of the $\mathrm{t\bar{t}}$ and di-boson backgrounds are estimated from simulation using MADGRAPH [41] and PYTHIA [42], respectively. The event yields are determined from measurements in background-enriched regions.

The event generator PYTHIA is used to model the MSSM Higgs boson signal. Taus are decayed

by the TAUOLA [43] package. In all Monte Carlo samples, additional interactions are simulated and reweighted to the observed pile-up distribution. The missing transverse energy in Monte Carlo simulated events is corrected for the difference between data and simulation measured using a sample of $Z \to \mu\mu$ events [44].

Table 1: Number of expected events in the two event categories in the $\mu\tau_h$ channel, where the combined statistical and systematic uncertainty is shown. The signal yields for the sum of all three neutral MSSM Higgs bosons, A+H+h, expected for M_A= 160 GeV and tan β= 8 are given for comparison. Also given are the products of signal efficiency times acceptance for M_Φ= 160 GeV.

Process	*B-Tag*	*No-B-Tag*
Z$\to \tau\tau$	1381 $\pm$ 103	112024 $\pm$ 7721
QCD	685 $\pm$ 113	22863 $\pm$ 1858
W+jets	291 $\pm$ 74	15552 $\pm$ 1299
Z+jets (l/jet faking τ)	63 $\pm$ 10	4232 $\pm$ 638
$t\bar{t}$	222 $\pm$ 36	678 $\pm$ 85
Dibosons	73 $\pm$ 10	623 $\pm$ 91
Total Background	2715 $\pm$ 175	155972 $\pm$ 8073
A+H+h $\to \tau\tau$	85 $\pm$ 6	1174 $\pm$ 61
Data	2761	159294
Signal Eff.		
gg$\to \Phi$	$2.36 \cdot 10^{-4}$	$1.91 \cdot 10^{-2}$
bb$\to \Phi$	$2.82 \cdot 10^{-3}$	$1.63 \cdot 10^{-2}$

Table 2: Number of expected events in the two event categories in the $e\tau_h$ channel, where the combined statistical and systematic uncertainty is shown. The signal yields for the sum of all three neutral MSSM Higgs bosons, A+H+h, expected for M_A= 160 GeV and tan β= 8 are given for comparison. Also given are the products of signal efficiency times acceptance for M_Φ= 160 GeV.

Process	*B-Tag*	*No-B-Tag*
Z$\to \tau\tau$	580 $\pm$ 43	41349 $\pm$ 2797
QCD	268 $\pm$ 41	14817 $\pm$ 1166
W+jets	157 $\pm$ 39	7534 $\pm$ 630
Z+jets (l/jet faking τ)	95 $\pm$ 14	8035 $\pm$ 1109
$t\bar{t}$	116 $\pm$ 20	353 $\pm$ 44
Dibosons	37 $\pm$ 5	283 $\pm$ 41
Total Background	1253 $\pm$ 75	72371 $\pm$ 3288
A+H+h $\to \tau\tau$	48 $\pm$ 3	605 $\pm$ 31
Data	1249	73332
Signal Eff.		
gg$\to \Phi$	$1.16 \cdot 10^{-4}$	$1.04 \cdot 10^{-2}$
bb$\to \Phi$	$1.61 \cdot 10^{-3}$	$8.52 \cdot 10^{-3}$

Table 3: Number of expected events in the two event categories in the $e\mu$ channel, where the combined statistical and systematic uncertainty is shown. The signal yields for the sum of all three neutral MSSM Higgs bosons, A+H+h, expected for M_A= 160 GeV and tan β= 8 are given for comparison. Also given are the products of signal efficiency times acceptance for M_Φ= 160 GeV.

Process	*B-Tag*	*No-B-Tag*
Z$\rightarrow \tau\tau$	826 $\pm$ 30	60897 $\pm$ 2013
QCD	158 $\pm$ 46	4887 $\pm$ 1289
$t\bar{t}$	1496 $\pm$ 156	2826 $\pm$ 279
Dibosons	373 $\pm$ 51	2962 $\pm$ 387
Total Background	2853 $\pm$ 173	71572 $\pm$ 2437
A+H+h $\rightarrow \tau\tau$	43 $\pm$ 2	585 $\pm$ 19
Data	2911	72721
Signal Eff.		
gg$\rightarrow \Phi$	$9.41 \cdot 10^{-5}$	$9.54 \cdot 10^{-3}$
bb$\rightarrow \Phi$	$1.41 \cdot 10^{-3}$	$8.18 \cdot 10^{-3}$

Table 4: Number of expected events in the two event categories in the $\mu\mu$ channel, where the combined statistical and systematic uncertainty is shown. The signal yields for the sum of all three neutral MSSM Higgs bosons, A+H+h, expected for M_A= 160 GeV and tan β= 8 are given for comparison. Also given are the products of signal efficiency times acceptance for M_Φ= 160 GeV.

Process	*B-Tag*	*No-B-Tag*
Z$\rightarrow \tau\tau$	133 $\pm$ 9	27083 $\pm$ 1610
Z$\rightarrow \mu\mu$	6654 $\pm$ 381	2448357 $\pm$ 98499
QCD	36 $\pm$ 8	1526 $\pm$ 128
$t\bar{t}$	412 $\pm$ 48	1047 $\pm$ 115
Dibosons	49 $\pm$ 12	5848 $\pm$ 1437
Total Background	7284 $\pm$ 385	2483861 $\pm$ 98523
A+H+h $\rightarrow \tau\tau$	11 $\pm$ 0.7	258 $\pm$ 11
Data	7167	2493540
Signal Eff.		
gg$\rightarrow \Phi$	$2.35 \cdot 10^{-5}$	$4.17 \cdot 10^{-3}$
bb$\rightarrow \Phi$	$3.94 \cdot 10^{-4}$	$3.97 \cdot 10^{-3}$

Table 5: Number of expected events in the two event categories in the $\tau_h\tau_h$ channel, where the combined statistical and systematic uncertainty is shown. The signal yields for the sum of all three neutral MSSM Higgs bosons, A+H+h, expected for M_A= 160 GeV and tan β= 8 are given for comparison. Also given are the products of signal efficiency times acceptance for M_Φ= 160 GeV.

Process	*B-Tag*	*No-B-Tag*
Z$\rightarrow \tau\tau$	52 $\pm$ 10	2165 $\pm$ 423
QCD	296 $\pm$ 104	19842 $\pm$ 6945
W+jets	16 $\pm$ 5	630 $\pm$ 189
Z+jets (l/jet faking τ)	2 $\pm$ 0.4	95 $\pm$ 19
$t\bar{t}$	14 $\pm$ 3	33 $\pm$ 7
Dibosons	4 $\pm$ 1	55 $\pm$ 16
Total Background	384 $\pm$ 104	22836 $\pm$ 6960
A+H+h $\rightarrow \tau\tau$	26 $\pm$ 5	296 $\pm$ 42
Data	381	23606
Signal Eff.		
gg$\rightarrow \Phi$	$1.12 \cdot 10^{-4}$	$8.28 \cdot 10^{-3}$
bb$\rightarrow \Phi$	$1.19 \cdot 10^{-3}$	$6.61 \cdot 10^{-3}$

3 Tau-pair invariant mass reconstruction

To distinguish the signal of Higgs bosons from the background, the tau-pair mass, $M_{\tau\tau}$, is reconstructed using a maximum likelihood technique [15]. The algorithm computes the tau-pair mass that is most compatible with the observed momenta of visible tau decay products and the missing transverse energy reconstructed in the event. Free parameters, corresponding to the missing neutrino momenta, are subject to kinematic constraints and are eliminated by marginalization. The algorithm yields a tau-pair mass distribution consistent with the true value and a resolution of 15-20%.

4 Systematic uncertainties

Various imperfectly known or simulated effects can alter the shape and normalization of the invariant mass spectrum. The main contributions to the normalization uncertainty include the uncertainty in the total integrated luminosity (4.5% for 2011 and 2.6% for 2012 data) [45], jet energy scale (2–5% depending on η and p_{T}), background normalization (Tables 1– 4), Z boson production cross section (2.5%) [44], lepton identification and isolation efficiency (1.0%), and trigger efficiency (1.0%). The tau-identification efficiency uncertainty is estimated to be 7% from an independent study done using a tag-and-probe technique [44] including the uncertainty of the trigger efficiency. The lepton identification and isolation efficiencies are stable as a function of the number of additional interactions in the bunch crossing in data and in Monte Carlo simulation. The b-tagging efficiency has an uncertainty of 10%, and the b-mistag rate is accurate to 30% [37]. Uncertainties that contribute to mass spectrum shape variations include the tau (3%), muon (1%), and electron (1.5%) energy scales. The effect of the uncertainty on the $\not\!\!E_{\mathrm{T}}$ scale, mainly due to pile-up effects, is incorporated by varying the mass spectrum shape as

described in the next section. The neutral MSSM Higgs production cross sections and the corresponding uncertainties are provided by the LHC Higgs Cross Section Group [46]. The cross sections have been obtained from the GGH@NNLO [47–51] and HIGLU [52, 53] programs for the gluon-fusion process. For the $b\bar{b} \to \Phi$ process, the four-flavor calculation [54, 55] and the five-flavor calculation as implemented in BBH@NNLO [56] have been combined using the Santander matching scheme [57]. Yukawa couplings for the m_h^{max} MSSM benchmark scenario have been calculated by FeynHiggs [58–60]. The uncertainties for the MSSM signal depends on tanβ and M_A and can amount up to 25%. The MSTW2008 proton distribution function is used, and the associated uncertainties range from 2-10%. The renormalization and factorization scale uncertainties amount to 5-25% in the gluon-fusion process and 8-15% in the associated-b process.

5 Results

To search for the presence of a Higgs boson signal in the selected events, a binned maximum likelihood fit is performed. The tau-pair invariant-mass spectrum is used as input for the fit in the eτ_h, $\mu\tau_h$, eμ and $\tau_h\tau_h$ final states. The sensitivity of the $\mu\mu$ channel is enhanced by fitting the two-dimensional distribution of tau-pair invariant-mass versus M_{vis}, the mass of the visible tau decay products, utilizing the fact that most of the large $Z \to \mu\mu$ background contributing to this channel is concentrated in the M_{vis} distribution within a narrow peak around the Z-mass. The fit is performed simultaneously for the five final states eτ_h, $\mu\tau_h$, eμ, $\mu\mu$ and $\tau_h\tau_h$ and the two event categories B-tag and no-B-tag. Systematic uncertainties are represented by nuisance parameters in the fitting process. Log-normal priors are assumed for the normalization parameters, and Gaussian priors for mass-spectrum shape uncertainties. The uncertainties that affect the shape of the mass spectrum, mainly those corresponding to the energy scales, are represented by nuisance parameters whose variation results in a continuous perturbation of the spectrum shape. In the regions of $M_{\tau\tau} > 150$ GeV, where the event statistic of the background templates is reduced, a fit of the form $f = \exp\left(-\frac{M_{\tau\tau}}{c_0 + c_1 \cdot M_{\tau\tau}}\right)$ is performed, and the uncertainties on the fit parameters c_0 and c_1 are propagated.

The signal expectation is determined in each point of the parameter space as follows:

- At each point of M_A and tanβ the mass, the gluon-fusion and associated-b production cross sections and the branching ratio to $\tau\tau$ are determined for h, H and A.
- For each neutral Higgs boson the expected reconstructed di-τ mass is obtained via "horizontal template morphing" [61], using as input the $M_{\tau\tau}$ shape templates of the nearest lower and upper mass–points for which Monte Carlo samples have been produced.
- The contributions of all three neutral Higgs boson are added using the corresponding cross sections times branching fraction.

Fig. 1 shows the distribution of the tau-pair mass for the five final states in the no-B-Tag category, which is more sensitive to the gluon-fusion production mechanism, compared with the background prediction. Fig. 2 shows the distribution of the tau-pair mass for the five final states in the B-Tag category, which enhances the sensitivity to the bb$\to \Phi$ production mechanism.

The invariant mass spectra show no clear evidence for the presence of a MSSM Higgs boson signal, therefore 95% CL upper bounds on tanβ as a function of the pseudoscalar Higgs boson mass M_A are set. The limits are computed using the modified Frequentist method [62].

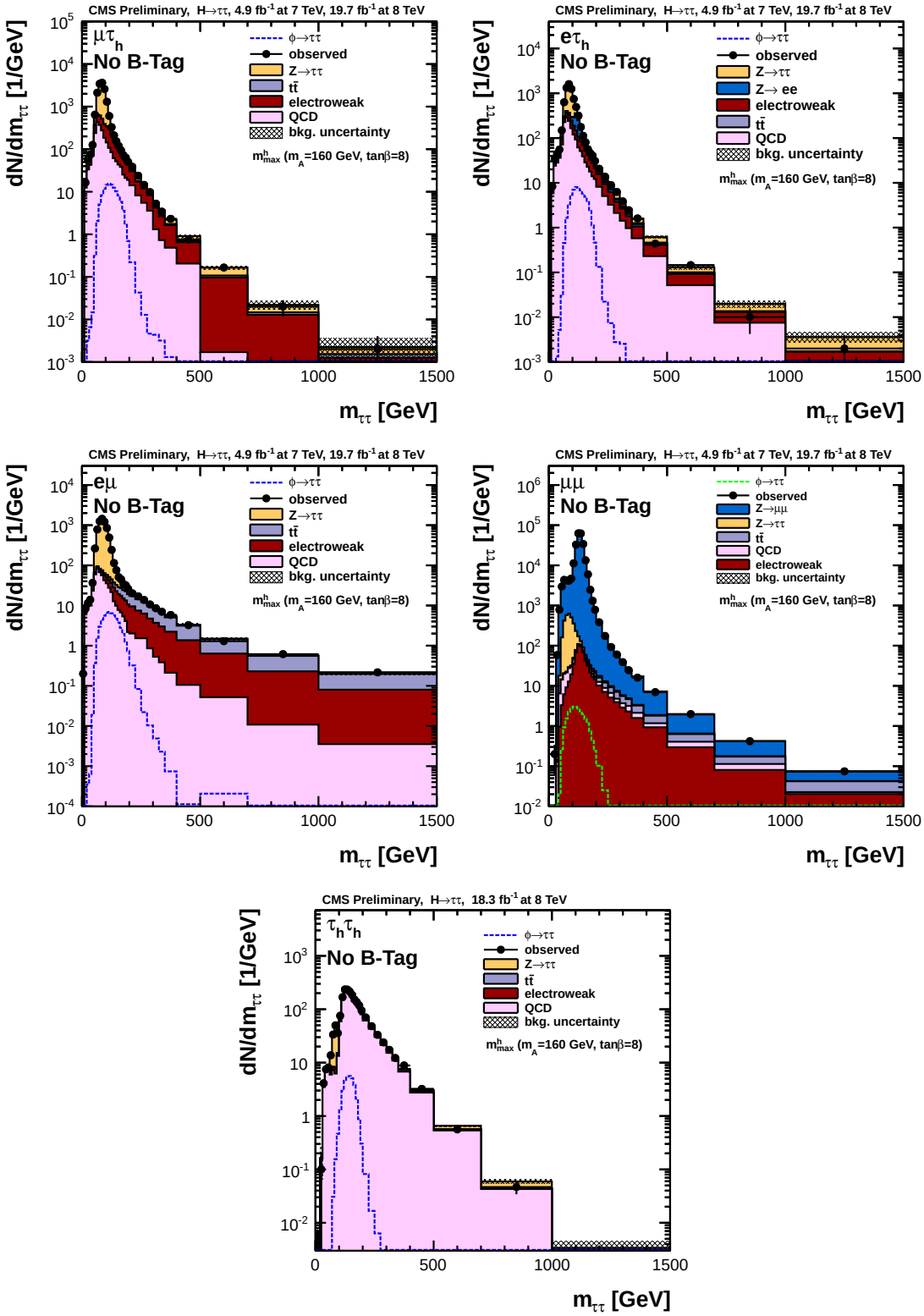

Figure 1: Reconstructed di-τ mass in the no-b-tag category for the $\mu\tau_h$, eτ_h, eμ, $\mu\mu$ and $\tau_h\tau_h$ channels.

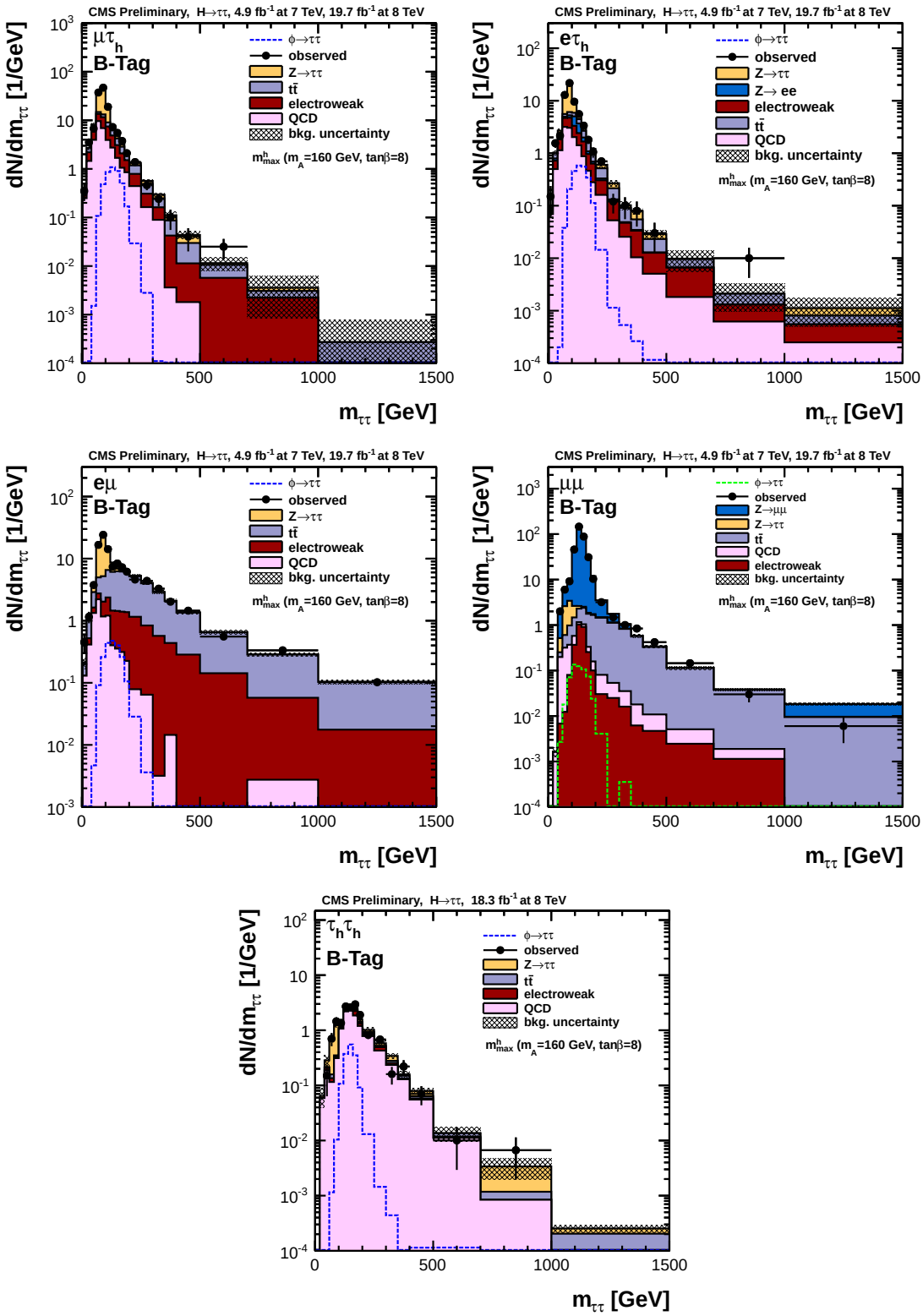

Figure 2: Reconstructed di-τ mass in the b-tag category for the $\mu\tau_h$, eτ_h, eμ, $\mu\mu$ and $\tau_h\tau_h$ channels.

Figure 3 shows the 95% CL exclusion in the tanβ-M_A parameter space for the MSSM m_h^{max} scenario. The exclusion limit set by the LEP experiments [20] is also shown. Numerical values for the expected and observed exclusion limits are given in Tab. 6. The expected limit has been computed for the case that no Higgs signal, neither of SM nor of MSSM type, is present in the data. The limit expected in case a SM Higgs boson is present in the data is computed separately and differs by 1-2 units in tanβ at low M_A. At high M_A there is also some effect as the limit is mainly driven by the light scalar Higgs h, which has the largest expected cross section.

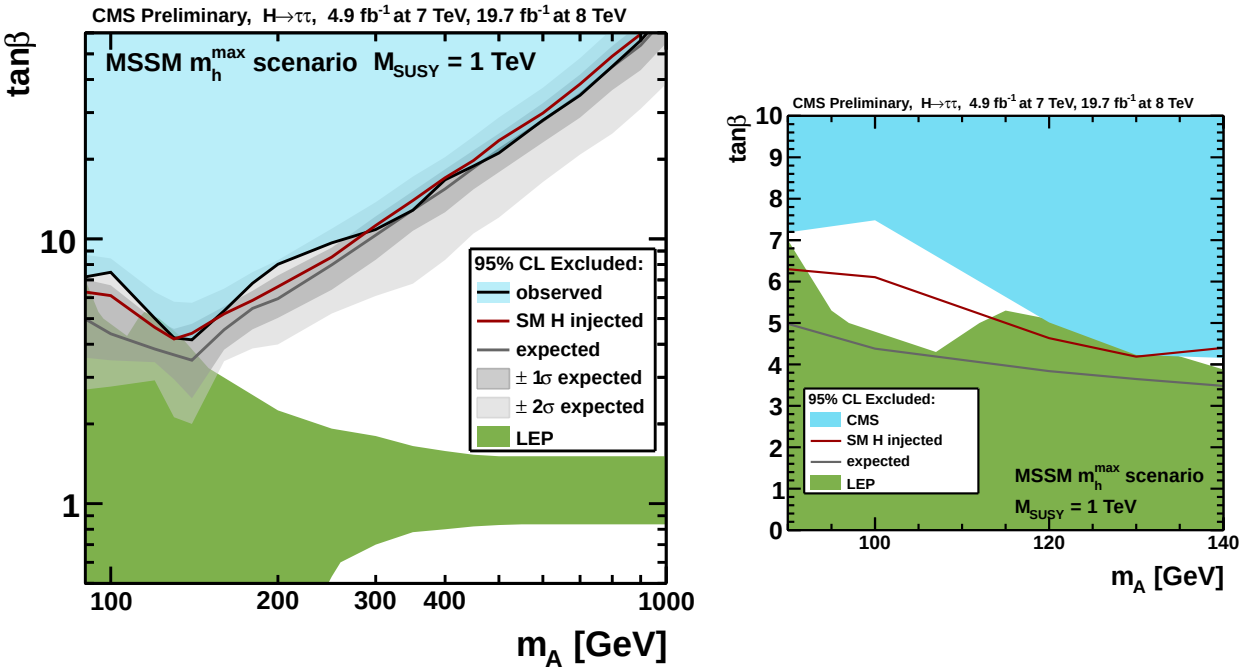

Figure 3: Left: Exclusion at 95% CL in the tanβ-M_A parameter space for the MSSM m_h^{max} scenario. The exclusion limits from the LEP experiments are also shown. Expected limits are computed for two cases: for the assumption that there is no Higgs $\rightarrow \tau\tau$ signal (neither MSSM nor SM) present in the data (dark grey line) and assuming that there is no MSSM, but a SM Higgs of mass 125–126 GeV present (red line). Right: 95% CL exclusion limit in the low M_A region.

Table 6: Expected range and observed 95% CL upper limits for $\tan\beta$ as a function of M_A, for the MSSM search.

MSSM Higgs	Expected $\tan\beta$ limit					Observed
m_{A} [GeV]	-2σ	-1σ	Median	$+1\sigma$	$+2\sigma$	$\tan\beta$ limit
90 GeV	2.70	3.56	4.98	7.02	8.71	7.19
100 GeV	2.77	3.48	4.38	6.68	8.44	7.48
120 GeV	2.92	3.42	3.84	4.94	6.30	5.01
130 GeV	2.12	2.95	3.65	4.57	5.79	4.23
140 GeV	2.00	2.50	3.48	4.78	5.74	4.16
160 GeV	3.45	3.81	4.54	5.56	6.49	5.35
180 GeV	3.86	4.55	5.46	6.36	7.49	6.80
200 GeV	3.99	5.03	5.95	7.28	8.32	8.02
250 GeV	5.22	6.43	7.98	9.27	10.9	9.66
300 GeV	6.09	8.34	10.3	12.2	13.8	10.9
350 GeV	6.77	10.7	12.9	15.1	17.2	12.8
400 GeV	8.33	12.6	15.4	18.3	20.4	16.7
450 GeV	10.5	15.4	18.5	21.6	24.4	18.8
500 GeV	12.0	17.9	21.7	25.0	28.8	21.1
600 GeV	16.4	23.1	27.9	32.6	37.2	28.1
700 GeV	20.8	28.7	35.2	41.8	48.2	34.9
800 GeV	25.0	36.5	44.7	53.6	> 60[1]	44.8
900 GeV	31.0	43.4	53.9	> 60 [1]	> 60 [1]	> 60 [1]
1000 GeV	38.5	54.9	> 60 [1]	> 60 [1]	> 60 [1]	> 60 [1]

[1] We do not quote limits above $\tan\beta = 60$ as the theoretical calculations which provide the relation between cross section and $\tan\beta$ become unreliable at high $\tan\beta$.

Model independent limits on $\sigma \cdot \mathrm{BR}(\Phi \to \tau\tau)$ for gluon-fusion and b-associated Higgs production as a function of the Higgs mass have been determined. The results for 8 TeV center-of-mass energy are shown in Fig. 4. In this case, a single resonance search (for a resonance of mass m_Φ) is performed. The results are also shown in Tables 7 and 8. Figures 5- 8 show the 2-dimensional 68% and 95% CL likelihood scans of $\sigma \cdot \mathrm{BR}(\Phi \to \tau\tau)$ for gluon-fusion and b-associated Higgs production, for different Higgs masses.

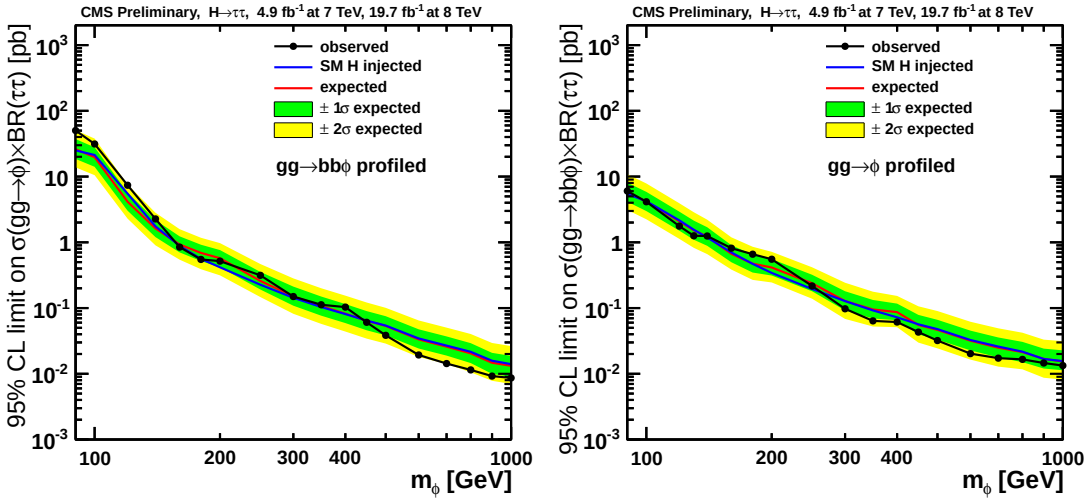

Figure 4: 95% CL upper limit on $\sigma \cdot \mathrm{BR}(\Phi \to \tau\tau)$ for gluon-fusion (left) and b-associated (right) production at 8 TeV center-of-mass energy as a function of M_Φ. Expected limits are computed for two cases: for the assumption that there is no Higgs $\to \tau\tau$ signal (neither MSSM nor SM) present in the data (red line) and assuming that there is no MSSM, but a SM Higgs of mass 125–126 GeV present (blue line).

Table 7: 95% CL upper limits for $\sigma\cdot$BR(ggΦ) (pb) as a function of M_Φ.

MSSM Higgs	Expected $\sigma\cdot$BR (ggΦ) limit					Observed
m_Φ [GeV]	-2σ	-1σ	Median	$+1\sigma$	$+2\sigma$	$\sigma\cdot$BR (ggΦ) limit
90 GeV	13.8	18.6	26.1	37.2	50.9	50.2
100 GeV	10.5	14.1	19.8	27.9	37.8	31.3
120 GeV	2.29	3.03	4.14	5.71	7.56	7.38
140 GeV	$8.99 \cdot 10^{-1}$	1.20	1.63	2.18	2.82	2.27
160 GeV	$5.44 \cdot 10^{-1}$	$7.02 \cdot 10^{-1}$	$9.26 \cdot 10^{-1}$	1.23	1.58	$8.45 \cdot 10^{-1}$
180 GeV	$3.90 \cdot 10^{-1}$	$5.19 \cdot 10^{-1}$	$6.91 \cdot 10^{-1}$	$9.19 \cdot 10^{-1}$	1.17	$5.49 \cdot 10^{-1}$
200 GeV	$3.14 \cdot 10^{-1}$	$4.17 \cdot 10^{-1}$	$5.73 \cdot 10^{-1}$	$7.62 \cdot 10^{-1}$	$9.73 \cdot 10^{-1}$	$5.17 \cdot 10^{-1}$
250 GeV	$1.47 \cdot 10^{-1}$	$1.91 \cdot 10^{-1}$	$2.59 \cdot 10^{-1}$	$3.54 \cdot 10^{-1}$	$4.67 \cdot 10^{-1}$	$3.15 \cdot 10^{-1}$
300 GeV	$8.18 \cdot 10^{-2}$	$1.09 \cdot 10^{-1}$	$1.51 \cdot 10^{-1}$	$2.12 \cdot 10^{-1}$	$2.83 \cdot 10^{-1}$	$1.50 \cdot 10^{-1}$
350 GeV	$5.74 \cdot 10^{-2}$	$7.65 \cdot 10^{-2}$	$1.07 \cdot 10^{-1}$	$1.50 \cdot 10^{-1}$	$2.00 \cdot 10^{-1}$	$1.12 \cdot 10^{-1}$
400 GeV	$4.39 \cdot 10^{-2}$	$5.91 \cdot 10^{-2}$	$8.20 \cdot 10^{-2}$	$1.15 \cdot 10^{-1}$	$1.54 \cdot 10^{-1}$	$1.03 \cdot 10^{-1}$
450 GeV	$3.43 \cdot 10^{-2}$	$4.59 \cdot 10^{-2}$	$6.41 \cdot 10^{-2}$	$8.99 \cdot 10^{-2}$	$1.21 \cdot 10^{-1}$	$6.07 \cdot 10^{-2}$
500 GeV	$2.88 \cdot 10^{-2}$	$3.84 \cdot 10^{-2}$	$5.34 \cdot 10^{-2}$	$7.52 \cdot 10^{-2}$	$1.01 \cdot 10^{-1}$	$3.85 \cdot 10^{-2}$
600 GeV	$1.80 \cdot 10^{-2}$	$2.42 \cdot 10^{-2}$	$3.34 \cdot 10^{-2}$	$4.75 \cdot 10^{-2}$	$6.48 \cdot 10^{-2}$	$1.93 \cdot 10^{-2}$
700 GeV	$1.42 \cdot 10^{-2}$	$1.89 \cdot 10^{-2}$	$2.59 \cdot 10^{-2}$	$3.70 \cdot 10^{-2}$	$5.04 \cdot 10^{-2}$	$1.43 \cdot 10^{-2}$
800 GeV	$1.05 \cdot 10^{-2}$	$1.46 \cdot 10^{-2}$	$2.04 \cdot 10^{-2}$	$2.92 \cdot 10^{-2}$	$4.03 \cdot 10^{-2}$	$1.15 \cdot 10^{-2}$
900 GeV	$7.82 \cdot 10^{-3}$	$9.98 \cdot 10^{-3}$	$1.47 \cdot 10^{-2}$	$2.08 \cdot 10^{-2}$	$2.94 \cdot 10^{-2}$	$9.23 \cdot 10^{-3}$
1000 GeV	$7.02 \cdot 10^{-3}$	$8.96 \cdot 10^{-3}$	$1.32 \cdot 10^{-2}$	$1.87 \cdot 10^{-2}$	$2.64 \cdot 10^{-2}$	$8.65 \cdot 10^{-3}$

Table 8: Expected range and observed 95% CL upper limits for $\sigma\cdot$BR(bbΦ) (pb) at 8 TeV center-of-mass energy as a function of M_Φ.

MSSM Higgs	Expected $\sigma\cdot$BR (bbΦ) limit					Observed
m_Φ [GeV]	-2σ	-1σ	Median	$+1\sigma$	$+2\sigma$	$\sigma\cdot$BR (bbΦ) limit
90 GeV	3.11	4.15	5.79	8.07	10.9	6.03
100 GeV	2.24	2.99	4.17	5.85	7.85	4.14
120 GeV	1.13	1.50	2.09	2.93	3.93	1.76
140 GeV	$6.61\cdot10^{-1}$	$8.85\cdot10^{-1}$	1.22	1.70	2.21	1.25
160 GeV	$3.85\cdot10^{-1}$	$4.98\cdot10^{-1}$	$6.68\cdot10^{-1}$	$9.05\cdot10^{-1}$	1.19	$8.14\cdot10^{-1}$
180 GeV	$2.68\cdot10^{-1}$	$3.47\cdot10^{-1}$	$4.73\cdot10^{-1}$	$6.49\cdot10^{-1}$	$8.56\cdot10^{-1}$	$6.59\cdot10^{-1}$
200 GeV	$2.45\cdot10^{-1}$	$3.12\cdot10^{-1}$	$4.14\cdot10^{-1}$	$5.54\cdot10^{-1}$	$7.17\cdot10^{-1}$	$5.53\cdot10^{-1}$
250 GeV	$1.39\cdot10^{-1}$	$1.80\cdot10^{-1}$	$2.38\cdot10^{-1}$	$3.21\cdot10^{-1}$	$4.17\cdot10^{-1}$	$2.17\cdot10^{-1}$
300 GeV	$6.84\cdot10^{-2}$	$9.20\cdot10^{-2}$	$1.28\cdot10^{-1}$	$1.80\cdot10^{-1}$	$2.43\cdot10^{-1}$	$9.75\cdot10^{-2}$
350 GeV	$5.24\cdot10^{-2}$	$6.94\cdot10^{-2}$	$9.52\cdot10^{-2}$	$1.33\cdot10^{-1}$	$1.77\cdot10^{-1}$	$6.38\cdot10^{-2}$
400 GeV	$5.12\cdot10^{-2}$	$6.53\cdot10^{-2}$	$8.67\cdot10^{-2}$	$1.17\cdot10^{-1}$	$1.53\cdot10^{-1}$	$6.13\cdot10^{-2}$
450 GeV	$2.98\cdot10^{-2}$	$3.98\cdot10^{-2}$	$5.53\cdot10^{-2}$	$7.87\cdot10^{-2}$	$1.06\cdot10^{-1}$	$4.31\cdot10^{-2}$
500 GeV	$2.44\cdot10^{-2}$	$3.30\cdot10^{-2}$	$4.66\cdot10^{-2}$	$6.62\cdot10^{-2}$	$9.01\cdot10^{-2}$	$3.20\cdot10^{-2}$
600 GeV	$1.64\cdot10^{-2}$	$2.27\cdot10^{-2}$	$3.19\cdot10^{-2}$	$4.53\cdot10^{-2}$	$6.19\cdot10^{-2}$	$2.03\cdot10^{-2}$
700 GeV	$1.29\cdot10^{-2}$	$1.78\cdot10^{-2}$	$2.49\cdot10^{-2}$	$3.57\cdot10^{-2}$	$4.92\cdot10^{-2}$	$1.73\cdot10^{-2}$
800 GeV	$1.17\cdot10^{-2}$	$1.50\cdot10^{-2}$	$2.14\cdot10^{-2}$	$3.06\cdot10^{-2}$	$4.21\cdot10^{-2}$	$1.66\cdot10^{-2}$
900 GeV	$8.70\cdot10^{-3}$	$1.20\cdot10^{-2}$	$1.69\cdot10^{-2}$	$2.41\cdot10^{-2}$	$3.31\cdot10^{-2}$	$1.46\cdot10^{-2}$
1000 GeV	$8.17\cdot10^{-3}$	$1.13\cdot10^{-2}$	$1.54\cdot10^{-2}$	$2.27\cdot10^{-2}$	$3.14\cdot10^{-2}$	$1.33\cdot10^{-2}$

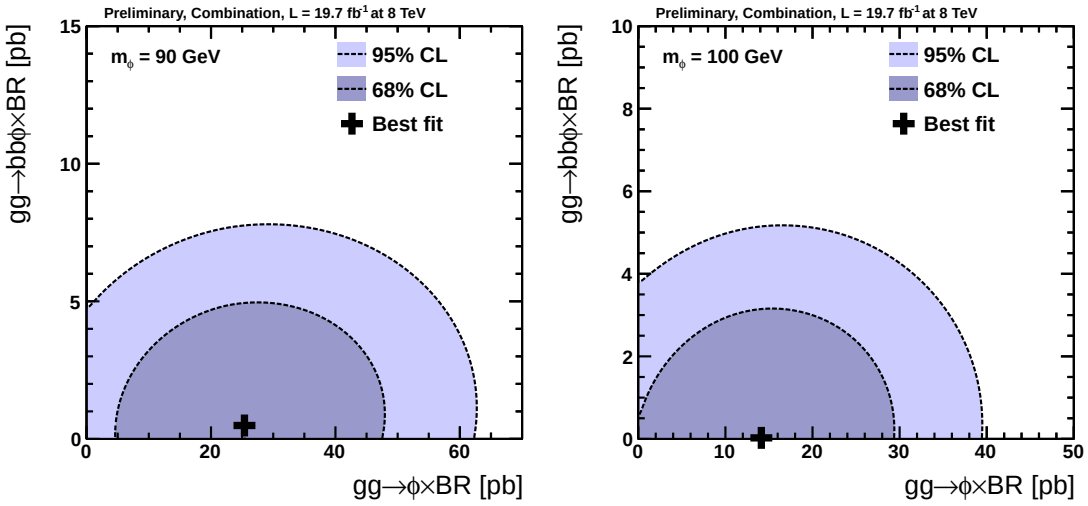

Figure 5: Likelihood contours of $\sigma\cdot$BR(ggΦ) and $\sigma\cdot$BR(bbΦ) at 8 TeV center-of-mass energy for different Higgs boson masses

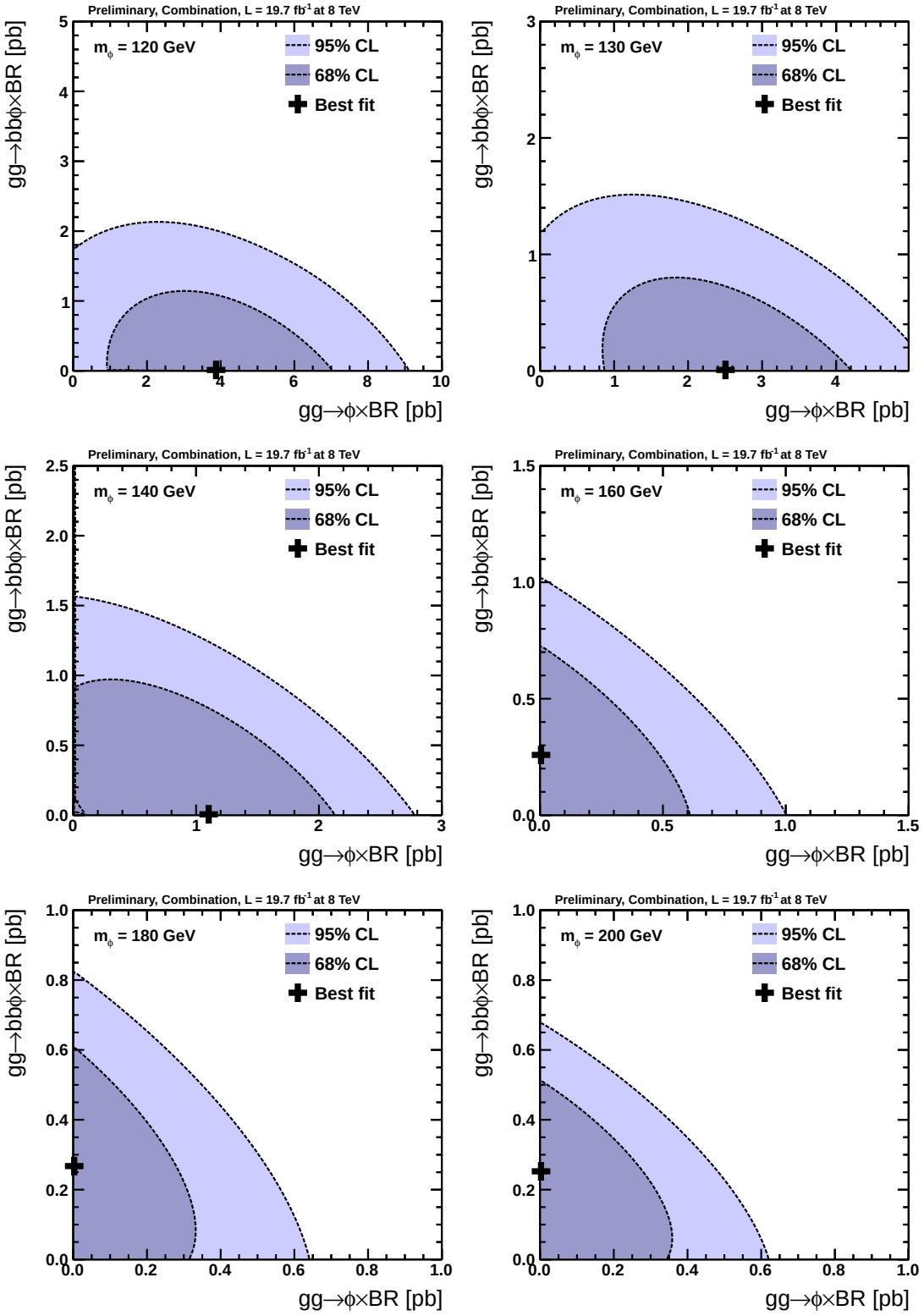

Figure 6: Likelihood contours of $\sigma \cdot \mathrm{BR}(\mathrm{gg}\Phi)$ and $\sigma \cdot \mathrm{BR}(\mathrm{bb}\Phi)$ at 8 TeV center-of-mass energy for different Higgs boson masses

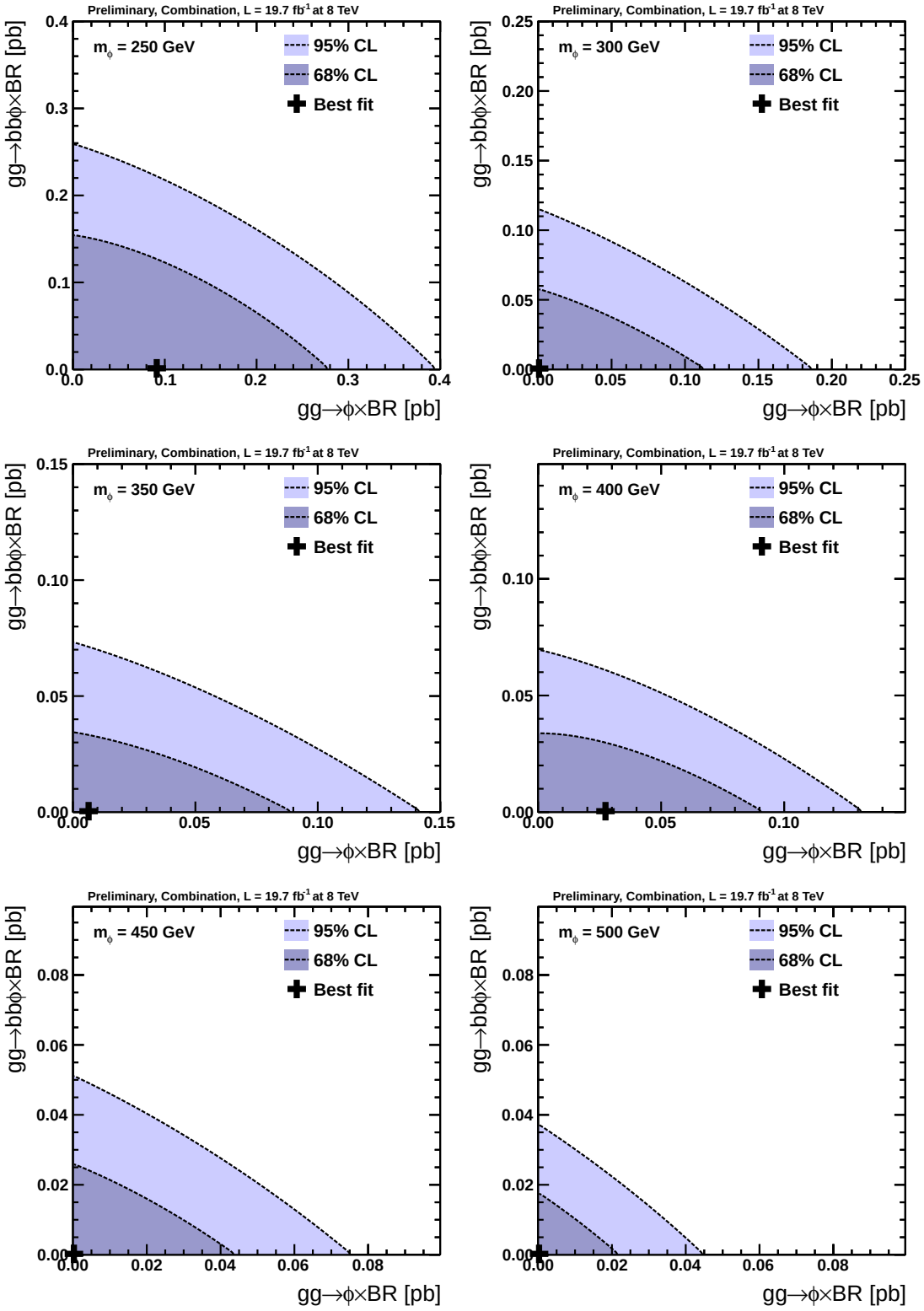

Figure 7: Likelihood contours of $\sigma\cdot$BR(ggΦ) and $\sigma\cdot$BR(bbΦ) at 8 TeV center-of-mass energy for different Higgs boson masses

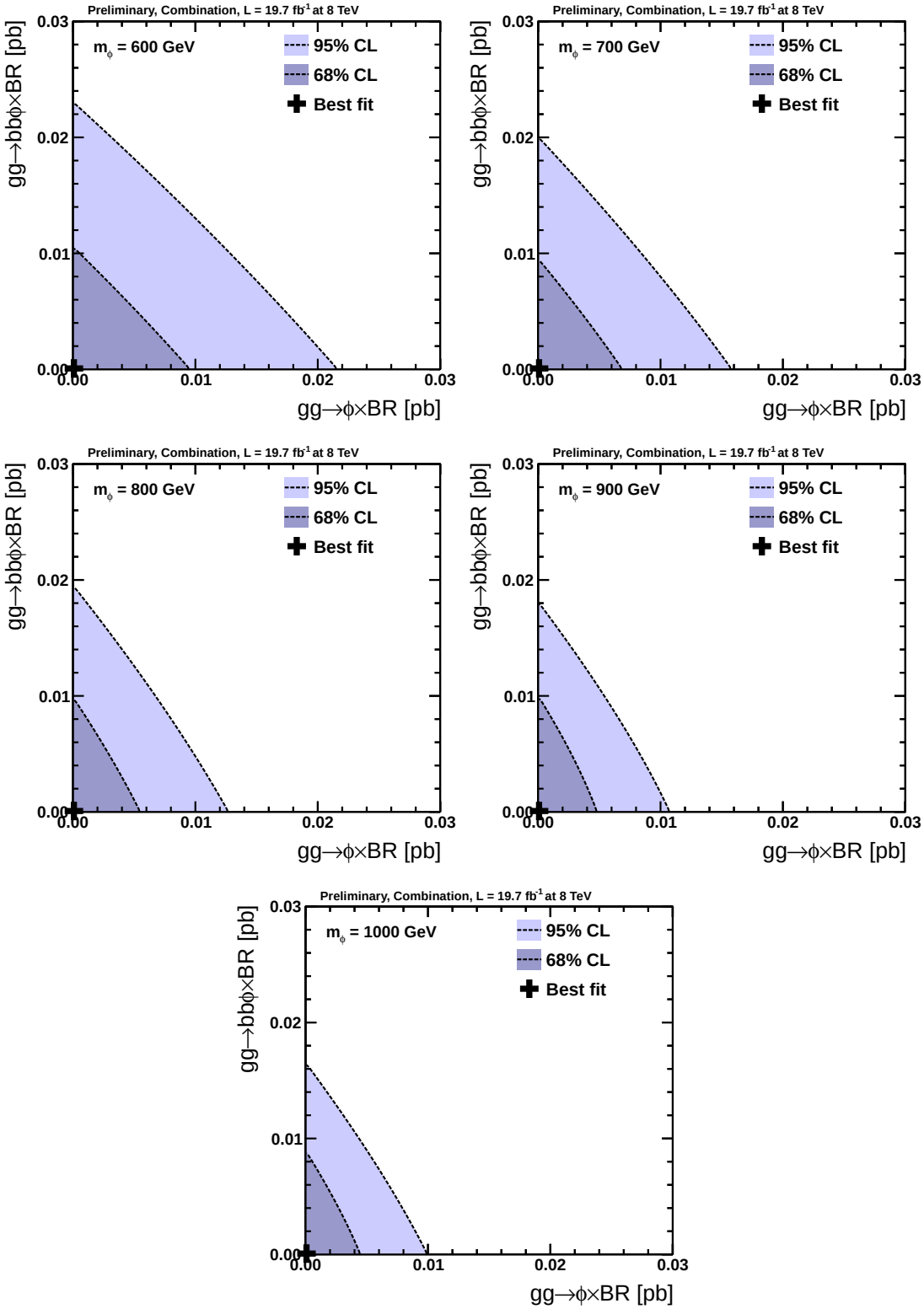

Figure 8: Likelihood contours of $\sigma\times$ BR(ggΦ) and $\sigma\times$ BR(bbΦ) at 8 TeV center-of-mass energy for different Higgs boson masses

6 Summary

A search for neutral Higgs bosons decaying to tau pairs has been performed using events recorded by the CMS experiment at the LHC in 2011 and 2012 at a center-of-mass energy of 7 TeV and 8 TeV respectively. The dataset corresponds to an integrated luminosity of 24.6 fb^{-1}, with 4.9 fb^{-1} at 7 TeV and 19.7 fb^{-1} at 8 TeV. Five different $\tau\tau$ final states are studied: $e\tau_h$, $\mu\tau_h$, $e\mu$, $\mu\mu$ and $\tau_h\tau_h$. To enhance the sensitivity to neutral Higgs bosons from the minimal supersymmetric extension of the standard model (MSSM), events containing zero and and events containing one b-tagged jet are analyzed in separate categories. No excess is observed in the tau-pair invariant-mass spectrum. Exclusion limits in the MSSM parameter space have been obtained for the m_h^{max} scenario. This search extends previous results to larger values of M_A and excluded values of tanβ as low as 4.2 at $M_A = 140$ GeV. Model independent upper limits on the Higgs boson production cross section times branching fraction for gluon-gluon fusion and b-associated production are also given.

References

[1] S. L. Glashow, "Partial Symmetries of Weak Interactions", *Nucl. Phys.* **22** (1961) 579, doi:10.1016/0029-5582(61)90469-2.

[2] S. Weinberg, "A Model of Leptons", *Phys. Rev. Lett.* **19** (1967) 1264, doi:10.1103/PhysRevLett.19.1264.

[3] A. Salam, "Weak and electromagnetic interactions", in *Elementary particle physics: relativistic groups and analyticity*, N. Svartholm, ed., p. 367. Almqvist & Wiskell, Stockholm, 1968. Proceedings of the eighth Nobel symposium.

[4] F. Englert and R. Brout, "Broken symmetry and the mass of gauge vector mesons", *Phys. Rev. Lett.* **13** (1964) 321, doi:10.1103/PhysRevLett.13.321.

[5] P. W. Higgs, "Broken symmetries, massless particles and gauge fields", *Phys. Lett.* **12** (1964) 132, doi:10.1016/0031-9163(64)91136-9.

[6] P. W. Higgs, "Broken symmetries and the masses of gauge bosons", *Phys. Rev. Lett.* **13** (1964) 508, doi:10.1103/PhysRevLett.13.508.

[7] G. S. Guralnik, C. R. Hagen, and T. W. B. Kibble, "Global conservation laws and massless particles", *Phys. Rev. Lett.* **13** (1964) 585, doi:10.1103/PhysRevLett.13.585.

[8] P. W. Higgs, "Spontaneous symmetry breakdown without massless bosons", *Phys. Rev.* **145** (1966) 1156, doi:10.1103/PhysRev.145.1156.

[9] T. W. B. Kibble, "Symmetry breaking in non-Abelian gauge theories", *Phys. Rev.* **155** (1967) 1554, doi:10.1103/PhysRev.155.1554.

[10] Y. Golfand and E. Likhtman, "Extension of the Algebra of Poincare Group Generators and Violation of p Invariance", *JETP Lett.* **13** (1971) 323–326.

[11] J. Wess and B. Zumino, "Supergauge Transformations in Four-Dimensions", *Nucl.Phys.* **B70** (1974) 39–50, doi:10.1016/0550-3213(74)90355-1.

[12] P. Fayet, "Supergauge invariant extension of the Higgs mechanism and a model for the electron and its neutrino", *Nucl. Phys. B* **90** (1975) 104, doi:10.1016/0550-3213(75)90636-7.

[13] P. Fayet, "Spontaneously broken supersymmetric theories of weak, electromagnetic and strong interactions", *Phys. Lett. B* **69** (1977) 489, doi:10.1016/0370-2693(77)90852-8.

[14] CMS Collaboration, "The CMS experiment at the CERN LHC", *JINST* **3** (2008) S08004, doi:10.1088/1748-0221/3/08/S08004.

[15] CMS Collaboration, "Search for neutral MSSM Higgs bosons decaying to tau pairs in pp collisions at $\sqrt{s} = 7$ TeV", *Phys. Rev. Lett.* **106** (2011) 231801, doi:10.1103/PhysRevLett.106.231801.

[16] ATLAS Collaboration, "Search for neutral MSSM Higgs bosons decaying to $\tau^+\tau^-$ pairs in proton-proton collisions at $\sqrt{s} = 7$ TeV with the ATLAS detector", *Phys. Lett. B* **705** (2011) 174, doi:10.1016/j.physletb.2011.10.001.

[17] CDF and D0 Collaborations, "Combined CDF and D0 Upper Limits on MSSM Higgs Boson Production in Tau-Tau Final States with up to 2.2 fb^{-1}", (2010). arXiv:hep-ex/1003.3363.

[18] D0 Collaboration, "Search for Higgs bosons decaying to $\tau^+\tau^-$ pairs in $p\bar{p}$ collisions at $\sqrt{s}$ = 1.96 TeV", *Phys. Lett. B* **707** (2012) 323, doi:10.1016/j.physletb.2011.12.050.

[19] CDF Collaboration, "Search for Higgs Bosons Predicted in Two-Higgs-Doublet Models via Decays to Tau Lepton Pairs in 1.96 TeV $p\bar{p}$ Collisions", *Phys. Rev. Lett.* **103** (2009) 201801, doi:10.1103/PhysRevLett.103.201801.

[20] LEP Collaborations ALEPH, DELPHI, L3 and OPAL Collaborations and the LEP Working Group for Higgs Boson Searches Collaboration, "Search for neutral MSSM Higgs bosons at LEP", *Eur. Phys. J. C* **47** (2006) 547, doi:10.1140/epjc/s2006-02569-7.

[21] M. S. Carena et al., "MSSM Higgs boson searches at the Tevatron and the LHC: Impact of different benchmark scenarios", *Eur. Phys. J. C* **45** (2006) 797, doi:10.1140/epjc/s2005-02470-y.

[22] M. S. Carena et al., "Suggestions for benchmark scenarios for MSSM Higgs boson searches at hadron colliders", *Eur. Phys. J. C* **26** (2003) 601, doi:10.1140/epjc/s2002-01084-3.

[23] CMS Collaboration Collaboration, "Observation of a new boson at a mass of 125 GeV with the CMS experiment at the LHC", *Phys.Lett.* **B716** (2012) 30–61, doi:10.1016/j.physletb.2012.08.021, arXiv:1207.7235.

[24] ATLAS Collaboration Collaboration, "Observation of a new particle in the search for the Standard Model Higgs boson with the ATLAS detector at the LHC", *Phys.Lett.* **B716** (2012) 1–29, doi:10.1016/j.physletb.2012.08.020, arXiv:1207.7214.

[25] CMS Collaboration, "Search for the Standard–Model Higgs boson decaying to tau pairs in proton–proton collisions at $\sqrt{s} = 7$ and 8 TeV", *CMS Paper in preparation* **CMS-PAPER-HIG-13-004** (2013).

[26] S. Heinemeyer, O. Stal, and G. Weiglein, "Interpreting the LHC Higgs Search Results in the MSSM", *Phys.Lett.* **B710** (2012) 201–206, doi:10.1016/j.physletb.2012.02.084, arXiv:1112.3026.

[27] M. Carena et al., "MSSM Higgs Boson Searches at the LHC: Benchmark Scenarios after the Discovery of a Higgs-like Particle", arXiv:1302.7033.

[28] CMS Collaboration, "Electron Reconstruction and Identification at $\sqrt{s} = 7$ TeV", CMS Physics Analysis Summary CMS-PAS-EGM-10-004, (2010).

[29] CMS Collaboration, "Performance of muon identification in pp collisions at $\sqrt{s} = 7$ TeV", CMS Physics Analysis Summary CMS-PAS-MUO-10-002, (2010).

[30] CMS Collaboration, "Measurement of Inclusive Z Cross Section via Decays to Tau Pairs in pp Collisions at $\sqrt{s}$=7 TeV", *JHEP* **8** (2011) 117, doi:10.1007/JHEP08(2011)117.

[31] CMS Collaboration, "Particle–Flow Event Reconstruction in CMS and Performance for Jets, Taus, and $E_{\mathrm{T}}^{\mathrm{miss}}$", CMS Physics Analysis Summary CMS-PAS-PFT-09-001, (2009).

[32] CMS Collaboration, "Commissioning of the Particle-Flow Reconstruction in Minimum-Bias and Jet Events from pp Collisions at 7 TeV", CMS Physics Analysis Summary CMS-PAS-PFT-10-002, (2010).

[33] CMS Collaboration, "Commissioning of the particle-flow event reconstruction with leptons from J/Ψ and W decays at 7 TeV", CMS Physics Analysis Summary CMS-PAS-PFT-10-003, (2010).

[34] M. Cacciari, G. P. Salam, and G. Soyez, "FastJet user manual",. arXiv:hep-ph/1111.6097v1.

[35] M. Cacciari and G. P. Salam, "Dispelling the N^3 myth for the k_t jet-finder", *Phys. Lett. B* **641** (2006) 57, doi:10.1016/j.physletb.2006.08.037, arXiv:hep-ph/0512210.

[36] CMS Collaboration, "Performance of tau-lepton reconstruction and identification in CMS", *JINST* **7** (2012) P01001, doi:10.1088/1748-0221/7/01/P01001.

[37] CMS Collaboration, "b-Jet Identification in the CMS Experiment", CMS Physics Analysis Summary CMS-PAS-BTV-11-004, (2012).

[38] CMS Collaboration, "Performance of Missing Transverse Momentum Reconstruction Algorithms in Proton–Proton Collisions at $\sqrt{s} = 8$ TeV with the CMS Detector", CMS Physics Analysis Summary CMS-PAS-JME-12-002, (2012).

[39] M. Cacciari and G. P. Salam, "Pileup subtraction using jet areas", *Phys. Lett. B* **659** (2008) 119, doi:10.1016/j.physletb.2007.09.077, arXiv:hep-ph/0707.1378.

[40] CMS Collaboration, "Determination of Jet Energy Calibration and Transverse Momentum Resolution in CMS", *JINST* **6** (2011) 11002, doi:10.1088/1748-0221/6/11/P11002.

[41] J. Alwall et al., "MadGraph/MadEvent v4: the new web generation", *JHEP* **09** (2007) 028, doi:10.1088/1126-6708/2007/09/028, arXiv:hep-ph/0706.2334.

[42] T. Sjöstrand, S. Mrenna, and P. Skands, "PYTHIA 6.4 physics and manual", *JHEP* **05** (2006) 026, doi:10.1088/1126-6708/2006/05/026.

[43] Z. Wąs, "TAUOLA the library for tau lepton decay, and KKMC/KORALB/KORALZ... status report", *Nucl. Phys. B, Proc. Suppl.* **98** (2001) 96, doi:10.1016/S0920-5632(01)01200-2.

[44] CMS Collaboration, "Measurement of Inclusive W and Z Cross Sections in pp Collisions $\sqrt{s}$=7 TeV", *JHEP* **1110** (2011) 132, doi:10.1007/JHEP01(2011)080.

[45] CMS Collaboration, "Measurement of CMS Luminosity", CMS Physics Analysis Summary CMS-PAS-EWK-10-004, (2010).

[46] LHC Higgs Cross Section Working Group, "Handbook of LHC Higgs Cross Sections: 1. Inclusive Observables", CERN Report CERN-2011-002, (2011).

[47] R. V. Harlander and W. B. Kilgore, "Next-to-next-to-leading order Higgs production at hadron colliders", *Phys. Rev. Lett.* **88** (2002) 201801, doi:10.1103/PhysRevLett.88.201801, arXiv:hep-ph/0201206.

[48] C. Anastasiou and M. Charalampos, "Higgs boson production at hadron colliders in NNLO QCD", *Nucl. Phys. B* **646** (2002) 220, doi:10.1016/S0550-3213(02)00837-4, arXiv:hep-ph/0207004.

[49] V. Ravindran, J. Smith, and W. L. van Neerven, "NNLO corrections to the total cross section for Higgs boson production in hadron hadron collisions", *Nucl. Phys. B* **665** (2003) 325, doi:10.1016/S0550-3213(03)00457-7, arXiv:hep-ph/0302135.

[50] R. V. Harlander and W. B. Kilgore, "Production of a pseudo-scalar Higgs boson at hadron colliders at next-to-next-to leading order", *JHEP* **10** (2002) 017, doi:10.1088/1126-6708/2002/10/017.

[51] C. Anastasiou and K. Melnikov, "Pseudoscalar Higgs boson production at hadron colliders in NNLO QCD", *Phys. Rev. D* **67** (2003) 037501, doi:10.1103/PhysRevD.67.037501, arXiv:hep-ph/0208115.

[52] M. Spira, A. Djouadi, D. Graudenz, and P. M. Zerwas, "Higgs boson production at the LHC", *Nucl. Phys. B* **453** (1995) 17, doi:10.1016/0550-3213(95)00379-7.

[53] M. Spira, "HIGLU: A Program for the Calculation of the Total Higgs Production Cross Section at Hadron Colliders via Gluon Fusion including QCD Corrections", arXiv:hep-ph/9510347.

[54] S. Dittmaier, M. Kramer, and M. Spira, "Higgs radiation off bottom quarks at the Tevatron and the LHC", *Phys. Rev. D* **70** (2004) 074010, doi:10.1103/PhysRevD.70.074010.

[55] S. Dawson, C. Jackson, L. Reina, and D. Wackeroth, "Exclusive Higgs boson production with bottom quarks at hadron colliders", *Phys. Rev. D* **69** (2004) 074027, doi:10.1103/PhysRevD.69.074027, arXiv:hep-ph/0311067.

[56] R. V. Harlander and W. B. Kilgore, "Higgs boson production in bottom quark fusion at next-to-next-to-leading order", *Phys. Rev. D* **68** (2003) 013001, doi:10.1103/PhysRevD.68.013001.

[57] R. Harlander, M. Kramer, and M. Schumacher, "Bottom-quark associated Higgs-boson production: reconciling the four- and five-flavour scheme approach", arXiv:hep-ph/1112.3478.

[58] S. Heinemeyer, W. Hollik, and G. Weiglein, "FeynHiggs: a program for the calculation of the masses of the neutral CP-even Higgs bosons in the MSSM", *Comput. Phys. Commun.* **124** (2000) 76–89, doi:10.1016/S0010-4655(99)00364-1.

[59] S. Heinemeyer, W. Hollik, and G. Weiglein, "The Masses of the neutral CP-even Higgs bosons in the MSSM: Accurate analysis at the two loop level", *Eur. Phys. J. C* **9** (1999) 343, doi:10.1007/s100529900006.

[60] G. Degrassi et al., "Towards high-precision predictions for the MSSM Higgs sector", *Eur. Phys. J. C* **28** (2003) 133, doi:10.1140/epjc/s2003-01152-2.

[61] A. L. Read, "Linear interpolation of histograms", *Nucl.Instrum.Meth.* **A425** (1999) 357–360, doi:10.1016/S0168-9002(98)01347-3.

[62] A. L. Read, "Modified frequentist analysis of search results (the CLs method)", CERN Report CERN-OPEN-2000-005, (2000).